LBL-29125
Preprint

Lawrence Berkeley Laboratory
UNIVERSITY OF CALIFORNIA

Accelerator & Fusion
Research Division

Submitted to Physical Review A

Transverse Resistive Wall Instability in the Two-Beam Accelerator

D.H. Whittum, A.M. Sessler, and V.K. Neil

June 1990

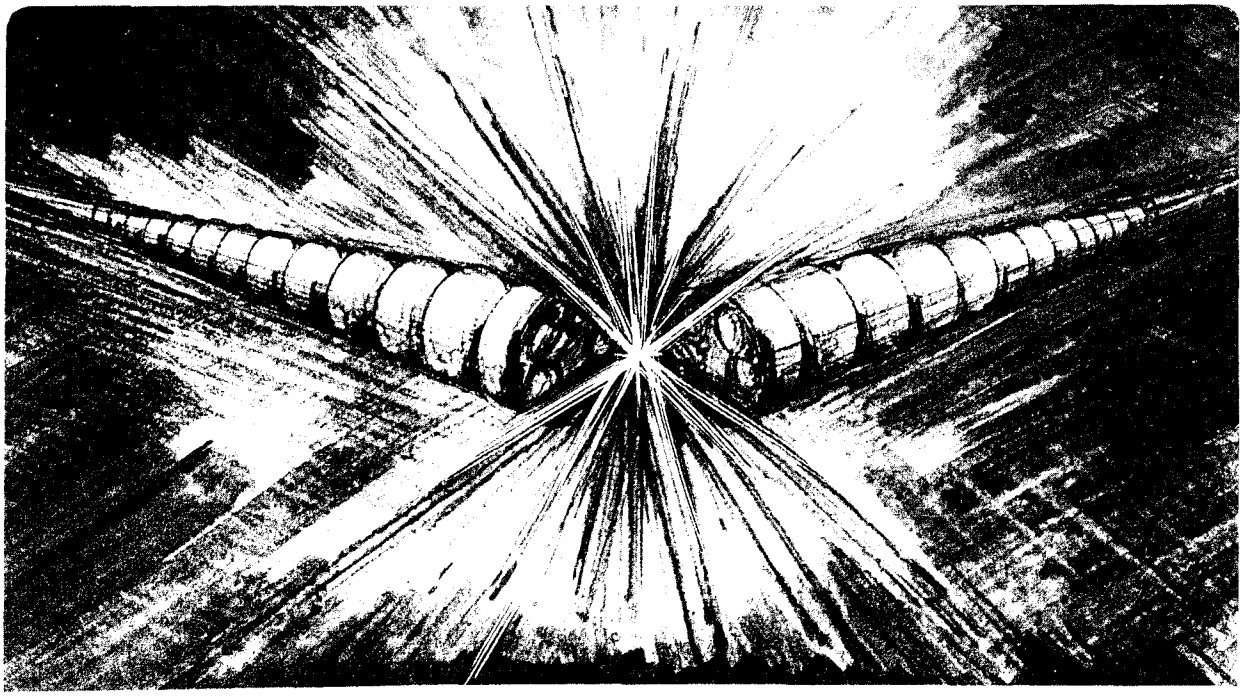

Prepared for the U.S. Department of Energy under Contract Number DE-AC03-76SF00098.

Transverse resistive wall instability in the two-beam accelerator

David H. Whittum and Andrew M. Sessler*
Lawrence Berkeley Laboratory,
University of California, Berkeley, California, 94720

V. Kelvin Neil**
Lawrence Livermore National Laboratory,
University of California, Livermore, California, 94550

*Work at LBL was supported by the Office of Energy Research, U.S. Dept. of Energy, under Contract No. DE-AC03-76SF00098.

**Work at LLNL was supported by DOE Contract No. W-7405-ENG-48, and by the Department of Defense under SDIO/SDC-ATC MIPR No. W31RPD-7-D4041.

Transverse resistive wall instability in the two-beam accelerator

David H. Whittum and Andrew M. Sessler

Lawrence Berkeley Laboratory, University of California, Berkeley, CA 94720

V. Kelvin Neil

Lawrence Livermore National Laboratory, University of California, Livermore, CA 94550

The transverse resistive wall instability in the Two-Beam Accelerator (TBA) is investigated analytically and numerically. Without any damping mechanism, we find one to four e-folds in 100 m, depending on the design. It is found that Landau damping, due to energy spread within a beam slice, is not effective, due to rapid synchrotron oscillations in the FEL ponderomotive well. Damping due to an energy sweep along the beam is also considered and it is found that a small variation in energy along the beam, decreasing from head to tail, can significantly reduce growth. We conclude that the resistive wall instability is not a severe design constraint on a TBA.

I. INTRODUCTION

The next generation of linear colliders will require accelerating gradients of 100 MeV/m or more to achieve TeV energies in a machine of reasonable length.[1,2] Such a gradient corresponds to an rf power of more than 100 MW produced per meter. A number of additional considerations, including the high luminosity requirement, alignment tolerances, bunch length requirements, final focus criteria, and rf breakdown thresholds conspire to constrain the range of operating frequencies for such a linac to 10-30 GHz.[1,3] In this range of frequency, the free-electron laser (FEL) and the relativistic klystron (RK) have demonstrated the power levels required,[4,5] and they have been proposed as microwave power sources for a TeV collider,[6,7] in a configuration dubbed the "Two-Beam Accelerator" (TBA).

In the TBA, a mildly relativistic, high current electron beam is transported through perhaps one-hundred FEL wigglers or RK cavities. This "drive" beam is alternately reaccelerated by induction cells, and deaccelerated through its interaction with the RK or FEL units. The microwave power is extracted and coupled into a slow-wave structure where it accelerates an extremely relativistic, low current electron beam. The conceptual layout of a single period of an FEL/TBA is depicted in Fig. 1.

Because of reacceleration, the TBA is capable of approaching 100% efficiency of conversion of beam power into rf power. It is this high efficiency, in addition to the practicality of using a proven power source, which motivates the TBA concept. However, there are a number of problems which arise due to reacceleration. These problems include drive beam loading due to the longitudinal wake of the induction cells,[8] rf phase-control,[9] rf extraction,[10] and transverse beam break-up (BBU) of the drive beam. Beam break-up is driven by the transverse wake of the induction cells,[11] and the wake of the resistive surfaces on the beam line (the pipe wall and the wiggler magnet pole faces).[12]

All of these issues have been addressed in detail elsewhere, except for the transverse resistive wall instability, the subject of this paper. In Sec. II we describe the model we use to study the instability, and we derive analytic results. In Sec. III, numerical results are exhibited, and, in Sec. IV, conclusions are offered. Detailed calculations are relegated to Appendices A and B. Table I lists the parameters we will consider for numerical examples.

II. TRANSVERSE RESISTIVE WALL INSTABILITY

A relativistic electron beam injected off-axis into a beamline will have an electrostatic dipole moment. The axial current associated with this dipole moment will couple to the axial electric fields of the various structures along the beamline. The associated transverse Lorentz force will give a kick to beam slices to the rear, displacing them farther off-axis. In this way, an instability obtains.

This "cumulative" beam break-up instability is described by an equation of the form[13]

$$\left(\frac{\partial}{\partial z}\gamma_i(\tau,z)\frac{\partial}{\partial z} + \gamma_i(\tau,z)\, k_{\beta i}^2(\tau,z)\right)\xi_i(\tau,z) = \int_0^s d\tau' \frac{I(\tau')}{I_A} W(\tau-\tau',z)\,\xi(\tau',z) \quad , \tag{1}$$

where $\tau=t-z/v_z$, indexes beam slices, $v_z\sim c$ is the axial beam velocity, and c is the speed of light. The integral extends from $\tau'=0$ (the beam head) to $\tau'=\tau$. The beam tail is located at $\tau=\tau_m$, with τ_m the pulse length. Beam electrons remain at a fixed τ, as they advance in z, down the beamline.

The beam current is $I(\tau)$ and will be assumed constant in τ ("d.c. beam").[14] $I_A=mc^3/e\sim 17$ kA is the Alfven current, where m is the electron mass and -e is its charge. $W(\tau-\tau')$, the wake potential,[15] is the Green's function which determines the

Lorentz force on an electron at a distance $v_z\tau$ from the beam head, as it arrives at z. This Lorentz force is due to the electric and magnetic fields generated by beam segments to the front --- i.e., with $\tau' < \tau$.

The term in the integrand is given by

$$\bar{\xi}(\tau',z) = \frac{1}{N}\sum_{i=1}^{N} \xi_i(\tau',z) \quad , \tag{2}$$

where the index i labels the N macroparticles (used to model beam electrons numerically) located at the same τ and z. $\xi_i(\tau,z)$, $\gamma_i(\tau,z)$, and $k_{\beta i}(\tau,z)$ are, respectively, the transverse displacement, Lorentz factor, and betatron wavenumber of the i-th macroparticle. (For a cold beam, where N=1, ξ_1 is just the beam centroid and will be denoted ξ.) Wiggler focussing is assumed.[16] The sum on the right side represents an average over the N macroparticles located in the slice at τ and z, and is proportional to the dipole moment of the axial current density.

Bodner, *et al.*,[17] have shown that, for a beam propagating down a smooth cylindrical pipe of radius b, with walls of conductivity, σ, the wake potential is given by[18]

$$W(\tau - \tau') \approx \frac{4}{\sqrt{\pi}} \frac{1}{\tau_D^{\nu 2}\, b^2} \frac{1}{\sqrt{\tau - \tau'}} \quad , \tag{3}$$

where $\tau_D = 4\pi\sigma b^2/c^2$.

This wake drives the "resistive wall instability" and arises from the diffusion of the dipole component of the beam magnetic field into the pipe. Caporaso, *et al.*,[19] have shown that, for a cold beam (N=1), the solution for the beam centroid is given asymptotically by,

$$\xi(\tau,z) \approx \frac{\theta(\tau)}{\sqrt{3\pi}} \frac{1}{(A/2)^{\nu 3}} \exp(Y_R) \sin(k_\beta z + Y_I) \quad , \tag{4}$$

where

$$Y_R = \frac{3}{2}(A/2)^{2/3} + \sqrt{3}\,\frac{(A/2)^{4/3}}{k_\beta z} - \frac{5}{3}\left(\frac{A}{k_\beta z}\right)^2 ,$$

$$Y_I = -\frac{3}{2}\sqrt{3}\,(A/2)^{2/3} - \frac{(A/2)^{4/3}}{k_\beta z} + \frac{2\pi}{3} , \qquad (5)$$

and

$$A = \left(\frac{I}{\gamma I_A}\right)\left(\frac{\tau}{\pi\sigma}\right)^{1/2}\left(\frac{cz}{k_\beta b^3}\right). \qquad (6)$$

This result assumes a constant beam energy, betatron wavelength, and pipe radius. In addition, in Eq. (5), certain corrections have been added to the result of Ref. 19, as derived in Appendix A.

The initial condition assumed in deriving Eqs. (4)-(5) is a unit displacement at z=0, i.e., $\xi(z=0,\tau)=\theta(\tau)$, where θ is the step function. A typical solution for $\xi(\tau,z)$, is depicted in Fig. 2, for b=1 cm. The envelope of ξ, will be denoted χ, and the maximum of χ, over all τ, at the TBA exit ($z=z_m$) will be referred to as the growth. Growth for z=100 m and a range of pipe radii is depicted in Fig. 3.

For simple estimates, growth may be taken to vary approximately as $\chi \sim \exp(z/L_g)^{2/3}$, with[20]

$$L_g = \frac{2^{7/2}}{3^{3/2}}\pi^{3/2}\frac{I_A}{I}\frac{\sigma^{1/2}}{\tau^{1/2}}\frac{\gamma b^3}{\lambda_\beta c} . \qquad (7)$$

From Eq. (7) it is evident that growth depends critically on the pipe radius, b, (the number of e-folds varies as $1/b^2$). This may also be seen by comparing Figs. 4(a) and 4(b), which depict $\xi(\tau,z)$ for b=1 cm and b=0.5 cm.

Evidently, control of BBU favors the largest b possible. On the other hand, b is constrained by the Halbach limit[21] which requires a narrow wiggler pole gap. (When the pole separation is large, the wiggler magnetic field strength is diminished.) Thus typical TBA designs[10] assume b in the range of 1 to 2 cm. From Eq. (4), this corresponds to BBU growth in the range of 4.5 to 0.5 e-folds, and this is acceptable. However, this analytic result will be modified by variations in energy within a beam slice, along the beam, and along the beamline. The need to incorporate such complicating effects motivates the numerical work of the next section.

III. NUMERICAL RESULTS

In this section, we examine numerical results from the code, "RWALL", which solves Eq. (1).[22] Numerical data are represented in Figs. 5-8 by solid dots and are interpolated smoothly. Each dot corresponds to one RWALL run and represents the maximum over all τ, of the centroid envelope, at z=100 m. In general, γ may vary according to

$$\gamma_i(\tau,z) = \bar{\gamma}(z) + \delta\gamma_i(\tau,z) \quad (8)$$

Eq. (10) states that the γ of the i-th macroparticle within the beam slice at τ, at position z, is given by the average beam γ at z, $\bar{\gamma}(z)$, plus a term corresponding to variation within a beam slice, along the beam, and along the beamline, $\delta\gamma_i(\tau,z)$. Four types of γ variation are of interest in a TBA.

A. Variation in γ due to reacceleration

The behavior of $\bar{\gamma}(z)$ in the TBA will be roughly a sawtooth. This is because energy is extracted over a TBA period, L ~ 1.3 m, via the FEL interaction, and then restored to the beam in a much shorter length of order millimeters to centimeters in crossing the induction cell gap. $\bar{\gamma}(z)$ is then modelled, for $0 < z < L$, by

$$\bar{\gamma}(z) = \gamma_+ (1 - \frac{z}{L}) + \gamma_-\left(\frac{z}{L}\right), \quad (9)$$

and this is extended periodically, with period L, and is independent of τ.

Growth for $(\gamma_+ + \gamma_-)/2 = 20$, with several different values of $\Delta\gamma = \gamma_+ - \gamma_-$, and with $\delta\gamma_i(\tau,z)=0$, is depicted in Fig. 5. For example, for $\Delta\gamma=1$, corresponding to a 5% sweep in γ through each period, growth is 4.51 e-folds, rather than 4.46, corresponding to a decrease in L_g by 1.5 % from 10.6 m to 10.4 m. Although the effect of this periodic variation in γ is to increase growth, the increase is fairly negligible, and we will hold $\bar{\gamma}$ constant in z for the remaining examples.

B.Spread in γ within a beam slice

High current electron beams typically have some spread in energy within a beam slice. Such a spread in γ within a beam slice may be modelled by

$$\delta\gamma_i(\tau,z) = \Delta\gamma \sin(\phi_i), \tag{10}$$

where $\Delta\gamma$ denotes the spread in values of γ and the ϕ_i are phases distributed uniformly from $-\pi$ to π. $\Delta\gamma$ and ϕ_i are independent of τ and z, so that $\delta\gamma_i(\tau,z)$ is also independent of τ and z. This spread in γ results in a spread in betatron periods among the macroparticles composing one beam slice. The centroid displacements of these macroparticles oscillating with different periods will then add incoherently in the wakefield driving term on the right side of Eq. (1) (phase-mixing). Intuitively, one expects that significant damping of growth will occur, provided the phase-mixing occurs in less than a growth length. If $\Delta k/k$ is the fractional spread in betatron wavenumbers and L_g is the growth length, the condition for phase-mix damping is then $\Delta k/k \sim \Delta\gamma/\gamma > 1/kL_g$.

This simple estimate agrees qualitatively with Fig. 6, which depicts resistive wall growth, with Landau damping. Evidently, even a small spread in energy can virtually eliminate growth. However, these considerations neglect the effect of synchrotron motion.

C. Synchrotron oscillations in γ

As the FEL signal power grows, electrons become trapped in the "ponderomotive well" of the signal field, and oscillate longitudinally, much as in an rf linac.[23] We model this synchrotron motion numerically by assuming all electrons are deeply trapped in the ponderomotive well and have a constant synchrotron period, so that

$$\delta\gamma_i(\tau,z) = \Delta\gamma \sin(k_{synch}\, z + \phi_i), \tag{11}$$

where $k_{synch}=2\pi/\lambda_{synch}$,[24] and $\Delta\gamma$ is the spread in values of γ. ϕ_i is the initial synchrotron phase (at the wiggler entrance) of the i-th macroparticle and the ϕ_i are distributed uniformly from $-\pi$ to π. Again, $\Delta\gamma$ and ϕ_i are independent of τ and z, so that $\delta\gamma_i(\tau,z)$ is independent of τ, but oscillates in z, with period λ_{synch}. If the synchrotron oscillations are rapid on the λ_β scale, then, on average, all particles will experience the same phase advance. Intuitively, one expects in this case that phase-

mixing will be negligible and that growth will not be damped. This effect was first investigated analytically by Takayama,[12] and is confirmed by Fig. 7, which depicts growth versus synchrotron period.

In Appendix B, we show that the condition for effective Landau damping with synchrotron motion is that $\Delta\gamma/\gamma$ be an appreciable fraction of $\lambda_\beta/\lambda_{synch}$.[25] This cannot be satisfied for typical TBA designs, since FEL efficiency requires a small spread in γ, within a slice, while its utility as a microwave source depends on a high output power, and therefore a short λ_{synch} (typically, $\lambda_\beta/\lambda_{synch} > 50\%$).

D. Sweep in γ along the beam

Previous work on energy and ponderomotive phase evolution through multiple TBA periods[9] indicates that a sweep in energy along the beam may arise in a natural way, due to variation in current along the beam. We model such a spread in γ along the beam by

$$\delta\gamma(\tau,z) = \Delta\gamma\left(\frac{\tau}{\tau_m} - \frac{1}{2}\right), \tag{12}$$

where $\Delta\gamma$ is the variation in γ from head to tail. Thus $\delta\gamma_i(\tau,z)$ is constant in z, but varies linearly in τ. Such a sweep in energy was first considered by Balakin, Novokhatsky and Smirnov (BNS) as a means of reducing growth of the beam break-up instability in linear accelerators.[26] For the long pulse considered here, this sweep produces phase-mixing from head to tail. Intuitively, one expects that phase-mixing in less than a growth length will reduce growth. This condition is $\Delta\gamma/\gamma > 1/kL_g$.

This expectation is confirmed in Fig. 8. A 2% sweep in γ along the length of the beam, decreasing toward the tail, reduces the growth from 4.5 e-folds to 2.3, corresponding to an increase in the growth length, L_g of 180%, from 10.5 m to 29.4 m. The dramatic effect of energy sweep is further illustrated by comparison of Figs. 9 and 2.

A striking feature of the BNS effect is the asymmetry in $\Delta\gamma$, first noted in Ref. 26. Growth is markedly reduced when the beam head is higher in energy than the tail ($\Delta\gamma<0$). For $\Delta\gamma>0$ growth actually increases for some range of z. Physically, this effect arises from a partial cancellation (reinforcement) of the wake driving term by the relativistic mass shift due to energy sweep, when $\Delta\gamma<0$ ($\Delta\gamma>0$) . However, for larger z, phase-mixing dominates, and growth will be reduced regardless of the sign of $\Delta\gamma$.[27]

In contrast to the condition for effective Landau damping, the condition for reduction in growth due to energy sweep is not stringent. In principle, BNS damping is achievable in an FEL, without degradation of efficiency. This may be understood by noting that the FEL instability is electromagnetic, and travels at a high group velocity, slipping little from a fixed beam slice. However, the resistive wall instability is cumulative, with zero group velocity. Efficiency of the FEL interaction depends on the quality (small energy spread) of the beam slice. The efficiency of the resistive wall instability depends on the quality and coherence of transverse motion of the beam as a whole. For the FEL, the effect of a sweep in energy is merely to cause the beam slices to sample different parts of the gain curve.

IV. CONCLUSIONS

From these examples, it is clear that the periodic variation in γ due to reacceleration will have little effect on resistive wall growth. In addition, the effect of Landau damping will be negligible due to rapid synchrotron motion. However, BNS damping does offer the possibility of reducing growth significantly. Further work is required to determine realistic energy sweeps consistent with the longitudinal dynamics of the FEL.

On the other hand, even without BNS damping, growth is tolerable, if non-negligible. For typical designs, we can expect from one to four e-folds in 100 m, depending largely on the pipe radius. BNS damping will reduce this even further.

ACKNOWLEDGEMENTS

Comments and instructive work on BBU by George J. Caporaso, Y. Y. Lau, Ronald R. Ruth, Henry D. Shay and Ken Takayama are greatly appreciated. Work at LBL was supported by the Office of Energy Research, U.S. Dept. of Energy, under Contract No. DE-AC03-76SF00098. Work at LLNL was supported by DOE Contract No. W-7405-ENG-48, and by the Department of Defense under SDIO/SDC-ATC MIPR No. W31RPD-7-D4041.

APPENDIX A:
ASYMPTOTIC GROWTH OF THE TRANSVERSE RESISTIVE WALL INSTABILITY

In Eq. (5), certain corrections have been added to the result of Ref. 19. In this Appendix, these corrections are derived. The motivation for this calculation is a discrepancy uncovered in comparing the numerical results of RWALL, and the analytic results of Ref. 19.

We begin with Eq. (10) of Ref. 19, the exact solution of Eq. (1), for the wake of Eq. (3),

$$\xi(\tau,z) = \theta(\tau)\frac{1}{4\pi i}\int_{-i\infty}^{i\infty} dp\,\frac{1}{p}\{\exp(f_+) + \exp(f_-)\}\,, \tag{A.1}$$

where p is the Laplace transform variable conjugate to τ, and the contour is to the right, in the complex p-plane, of all poles of the integrand. Other notation is

$$\begin{aligned} f_\pm(p) &= pA^2 \pm iBg(p)\,, \\ g(p) &= \sqrt{1-\frac{2}{Bp^{1/2}}}\,, \\ B &= k_\beta z\,, \end{aligned} \tag{A.2}$$

and A is defined in Eq. (6).

We proceed to calculate the integral of Eq. (A.1), using steepest descents. We set $f'_\pm(p)=0$ to find the stationary points, p_r,

$$A^2 \pm \frac{i}{2g(p_r)p_r^{3/2}} = 0\,, \tag{A.3}$$

or

$$p_r = \frac{r}{\left[2A^2 g(p_r)\right]^{2/3}}\,, \tag{A.4}$$

where, r= exp(iπ/3), exp(-iπ/3) and exp(iπ). Eq. (A.4) is a sixth-order polynomial for $p_r^{1/2}$. We approximate the roots by expanding them in the small parameter $\varepsilon=(4A)^{2/3}/B$. This expansion converges provided $\varepsilon<<1$, which is always true for sufficiently large z, since ε varies as $z^{-1/3}$. However, it is necessary to keep terms through the third order in ε, as will become apparent shortly.

Iteration of Eq. (A.4) gives

$$
\begin{aligned}
p_r &= \frac{r}{(2A^2)^{2/3}}\left\{1+\frac{\tilde{\varepsilon}}{3}+\frac{\tilde{\varepsilon}^2}{6}-\frac{\tilde{\varepsilon}^3}{81}+\dots\right\},\\
g(p_r) &= 1-\frac{\tilde{\varepsilon}}{2}-\frac{\tilde{\varepsilon}^2}{24}+\frac{7}{48}\tilde{\varepsilon}^3+\dots,\\
f_{\pm}(p_r) &= r\left(\frac{A}{2}\right)^{2/3}\left\{-\frac{4}{\tilde{\varepsilon}}+3+\frac{\tilde{\varepsilon}}{2}-\frac{5}{12}\tilde{\varepsilon}^2+\dots\right\},\\
f''_{\pm}(p_r) &= \frac{A^{10/3}}{r\,2^{4/3}}\left\{6-\tilde{\varepsilon}+\frac{\tilde{\varepsilon}^2}{6}+\dots\right\},
\end{aligned}
\qquad \text{(A.5)}
$$

where $\tilde{\varepsilon}=\varepsilon/r^{1/2}=\pm\varepsilon ir$. Only the roots $p_\pm$, corresponding to $r=\exp(\pm i\pi/3)$ contribute to the steepest descent calculation. We use the contour of Fig. 3, Ref. 19, and obtain

$$
\int_C dp\,\frac{1}{p}\exp\{f_{\sigma_1}\} \approx \sum_{\sigma_2=\pm1}\sqrt{\frac{2\pi}{\left|f''_{\sigma_1}(p_{\sigma_2})\right|}}\,\frac{1}{p_{\sigma_2}}\exp\{f_{\sigma_1}(p_{\sigma_2})+i\mu(p_{\sigma_2})\}
\qquad \text{(A.6)}
$$

where $\mu(p_\pm)=(\pi - \arg f''(p_\pm))/2$, or $\mu(p_+)=2\pi/3$ and $\mu(p_-)=\pi/3$.

We substitute Eq. (A.6) into Eq. (A.1) and take all quantities to lowest order in ε, except in the exponent. Eq. (A.1) becomes,

$$
\begin{aligned}
\xi(\tau,z) = \frac{\theta(\tau)}{4\pi i}\,\frac{\pi^{1/2}2^{4/3}}{3^{1/2}A^{1/3}}\Big\{&\exp[f_+(p_+)+i\pi/3]+\exp[f_-(p_+)+i\pi/3]\\
&\longrightarrow +\exp[f_+(p_-)+i2\pi/3]+\exp[f_-(p_-)+i2\pi/3]\Big\},
\end{aligned}
\qquad \text{(A.7)}
$$

where,

$$f_{\sigma_1}(p_{\sigma_2}) = \left(\frac{A}{2}\right)^{2/3} \left\{ \frac{4i}{\varepsilon}\sigma_1 + 3\exp[i\sigma_2\pi/3] \right.$$

$$\left. \longrightarrow -\frac{i\sigma_1\varepsilon}{2}\exp[-i\sigma_2\pi/3] - \frac{5}{12}\varepsilon^2 + \ldots \right\}, \qquad \text{(A.8)}$$

with $\sigma_1=\pm1$, $\sigma_2=\pm1$.

Evidently, we may drop the last two terms in Eq. (A.8), if we are interested only in the leading order growth in

$$\ln(\xi) \approx z^{2\beta}\left\{1 + O(\frac{1}{z^{1/3}}) + O(\frac{1}{z^{2\beta}}) + \ldots\right\}, \qquad \text{(A.9)}$$

and this is the approximation of Ref. 19. However, to accurately estimate the absolute magnitude of ξ, we must keep the $z^{1/3}$ and constant terms in the exponent. The final result is, after some algebra,

$$\xi(\tau,z) = \frac{\theta(\tau)}{\sqrt{3\pi}} \frac{1}{(A/2)^{\nu/3}} \exp(Y_R)\sin(k_\beta z + Y_I), \qquad \text{(A.10)}$$

where

$$Y_R = \frac{3}{2}(A/2)^{2/3} + \underbrace{\sqrt{3}\,\frac{(A/2)^{4/3}}{k_\beta z} - \frac{5}{3}(\frac{A}{k_\beta z})^2}_{\text{correction}},$$

$$Y_I = -\frac{3}{2}\sqrt{3}\,(A/2)^{2/3} \underbrace{-\frac{(A/2)^{4/3}}{k_\beta z}}_{\text{correction}} + \frac{2\pi}{3}, \qquad \text{(A.11)}$$

Eqs. (A10) and (A11) are just Eqs. (4) and (5). The uncorrected result of Ref. 19 is compared to the numerical result in Fig. A1 (a), and the corrected result is compared to the numerical result in Fig. A1 (b). Evidently the corrections are significant and produce good agreement with the numerical result.

To clarify the origin of these corrections, we consider the solution to Eq. (1) in the absence of energy spread, or acceleration

$$\xi(\tau,z) = \frac{1}{2\pi i}\int_{-i\infty+0^+}^{+i\infty+0^+} dp\ \frac{1}{p}\exp(p\tau)\cos\left\{k_\beta z\sqrt{1-\frac{I}{I_A}\frac{W(p)}{\gamma k_\beta^2}}\right\}, \tag{A.12}$$

where W(p) is the Laplace transform of the wake (the "impedance"). The approximation of Ref. 19 corresponds to an expansion of the square root keeping only the term of first order in W. (This is equivalent to the strong focussing approximation). In general, this is accurate only in the sense that the ratio of the logarithm of the analytic amplitude to the logarithm of the actual amplitude approaches 1 for large z. For full accuracy (so that the ratio of the amplitudes converges) more terms must be kept. For example, for $W(p) \propto p^{-r}$, $[r^{-1}+1]$ terms must be kept for full accuracy, where [x] is the greatest integer less than or equal to x. In the case that $r^{-1}+1$ is an integer, the last term will be independent of z.

APPENDIX B:
EFFECT OF SYNCHROTRON MOTION ON LANDAU DAMPING

In this Appendix, the condition for effective Landau damping in the presence of synchrotron motion is derived. We start from the Eq. (1) and express the center of mass displacement of the i-th macroparticle, ξ_i, in terms of a complex amplitude or eikonal, χ_i,

$$\xi_i(\tau,z) = \Im\left\{\chi_i(\tau,z)\ \exp\left(i\int_0^z k_{\beta i}\,dz'\right)\right\}. \tag{B.1}$$

We assume that the synchrotron oscillations are not fast on the scale of a betatron wavelength $k_{synch}<k_\beta$, and that the growth length satisfies $L_g > \lambda_\beta$. (the "strong focussing" approximation). In this case, the macroparticle eikonal χ_i varies slowly on the λ_β length scale and satisfies

$$2\,i\,\gamma_0 k_0 \frac{\partial\chi_i}{\partial z}(\tau,z) = \frac{I}{I_A}\int_0^\tau ds'\ W(\tau-\tau')\left\langle \chi_j(\tau',z)\exp\left(i\int_0^z (k_{\beta j}-k_{\beta i})\,dz'\right)\right\rangle_j \tag{B.2}$$

where $\langle\rangle_j$ indicates an average over j. Since $k_{\beta i}$ does not vary in τ, we may Laplace transform in τ to find

$$2\,i\,\gamma_0 k_0 \frac{\partial\chi_i}{\partial z}(p,z) = \frac{I}{I_A}\ W(p)\left\langle \chi_j(p,z)\exp\left(i\int_0^z (k_{\beta j}-k_{\beta i})dz'\right)\right\rangle_j. \tag{B.3}$$

Next, we replace the discrete index i, with a continuous phase variable ϕ, in which particles are uniformly distributed and take $k_\beta(\phi)=k_0+\Delta k\sin(k_0 z+\phi)$, abbreviating k_{synch} by k_s. Equation (B.3) then reduces to

$$\frac{\partial \chi_i}{\partial z}(z,\phi) = \frac{1}{2i\gamma_0 k_0}\frac{I}{I_A}\, W \frac{1}{2\pi}\int_{-\pi}^{\pi} d\phi' \chi(z,\phi') \rightarrow \exp\left(i\int_0^z \Delta k\,(\sin(k_s z' + \phi') - \sin(k_s z' + \phi))\, dz' \right), \tag{B.4}$$

where the variable, p, is suppressed for brevity, and we have used the fact that $k_\beta \gamma = k_0 \gamma_0$ is the same for each particle.[16] Eq. (B.4) then simplifies to

$$\frac{\partial \chi_i}{\partial z}(z,\phi) = \frac{1}{2i\gamma_0 k_0}\frac{I}{I_A}\, W \frac{1}{2\pi}\int_{-\pi}^{\pi} d\phi' \chi(z,\phi') \rightarrow \exp\left(2i\frac{\Delta k}{k_s}\sin\left(\frac{k_s z}{2}\right)\left(\sin\left(\frac{k_s z}{2} + \phi'\right) - \sin\left(\frac{k_s z}{2} + \phi\right)\right)\right). \tag{B.5}$$

Expanding χ in a Fourier series in ϕ,

$$\chi(z,\phi) = \sum_m y_m(z) \exp(im\phi), \tag{B.6}$$

it is straightforward to show that the Fourier coefficients y_m satisfy,

$$\frac{dy_m}{dz} = \left(\frac{1}{2i\gamma_0 k_0}\frac{I}{I_A}\, W\right)\sum_n J_m(\eta)\, J_n(\eta)\, y_n(z) \exp\left(i(m-n)\frac{k_s z}{2}\right), \tag{B.7}$$

where $\eta = 2(\Delta k/k_s)\sin(k_s z/2)$.

Next, we specialize to the case $k_s z >> 1$. In this limit, the harmonics y_m are decoupled, due to the rapid rotation in phase represented by the $k_s z$ term in Eq. (B.7). Since $y_{m\neq 0} << y_0$ at $z=0$, the $y_{m\neq 0}$ are small for all z and

$$y_0(z) \approx y_0(0) \exp\left(\frac{1}{2i\gamma_0 k_0}\frac{I}{I_A}\, W \int_0^z dz' J_0^2\left(2\frac{\Delta k}{k_s}\sin\left(\frac{k_s z}{2}\right)\right)\right). \tag{B.8}$$

Assuming $\Delta k/k_s << 1$, this simplifies to

$$y_0(z) = y_0(0) \exp\left(\frac{1}{2i\gamma_0 k_0}\frac{I}{I_A}\, W z\left[1 - \left(\frac{\Delta k}{k_s}\right)^2\left(1 - \frac{\sin(k_s z)}{k_s z}\right)\right]\right), \tag{B.9}$$

Noting that $\chi \sim y_0$, the solution for the envelope of the centroid motion is,

$$\chi(p,z) \approx \chi(0,z)\exp\left(\frac{1}{2\,i\,\gamma_0 k_0}\frac{I}{I_A}\,W(p)\,z\left[1-\left(\frac{\Delta k}{k_s}\right)^2\right]\right), \tag{B.10}$$

and the p-dependence has been restored for clarity.

From Eq. (B.10), it is evident that the cold-beam steepest descents calculation for the amplitude $\chi(\tau,z)$ goes through, yielding the usual asymptotic growth, except that z/L_g is replaced by z/L'_g where

$$L'_g = L_g \frac{1}{1-\left(\frac{\Delta k}{k_s}\right)^2}, \tag{B.11}$$

with L_g as defined in Eq. (7).

This result is quite general and applies to BBU due to an *arbitrary wake*. Growth as computed from Eq. (4), with L_g' substituted for L_g, is depicted in Fig. B1, together with the numerical data. Agreement is good, with a noticeable discrepancy as λ_s approaches L, and the $k_s z >> 1$ approximation breaks down.

[1]R. B. Palmer, *New Developments in Particle Acceleration Techniques*, CERN Report No. 87-11, ECFA 87/110 (CERN, Geneva, 1987) pp. 80-120.

[2]The present state of the art for rf linacs is about 20 MeV/m, at the Stanford Linear Collider. J.T. Seeman and J.C. Sheppard, Ref. 1, pp.122-133.

[3]P.B. Wilson, *Laser Acceleration of Particles*, edited by Chan Joshi and Thomas Katsouleas, AIP Conf. Proc. **130**, (AIP, New York, 1985) pp. 560-597.

[4] T.J. Orzechowski, *et al.*, Phys. Rev. Lett. **54**, 889 (1985).

[5] M. A. Allen, *et al.*, Phys. Rev. Lett **63**, 2472 (1989).

[6] A. M. Sessler, E. Sternbach, J. S. Wurtele, Nucl. Instrum. Methods **B40/41**, 1064 (1989).

[7]A. M. Sessler and S. S. Yu, Phys. Rev. Lett. **58**, 2439 (1987).

[8]D. H. Whittum, A. M. Sessler, G. Craig, J. DeFord and D. U. L. Yu,*Advanced Accelerator Concepts*, edited by Chan Joshi, AIP Conf. Proc. **193**, (AIP, New York, 1989) pp. 433-447.

[9]A. M. Sessler, D. H. Whittum and J. S. Wurtele, Particle Accelerators **31**, 1277 (1990).

[10]D. B. Hopkins, K. Halbach, E. H. Hoyer, A. M. Sessler, and E. J. Sternbach, Ref. 8, pp. 141-151.

[11]D. H. Whittum, G. A. Travish, A. M. Sessler, J. DeFord and G. Craig, *Proceedings of the 1989 IEEE Particle Accelerator Conference*, (Chicago, 1989) pp. 1190-1192.

[12]K. Takayama, Phys. Rev. A **39**, 184 (1989).

[13]K. L. F. Bane, *Physics of Particle Accelerators*, AIP Conf. Proc No. **153**, edited by Melvin Month and Margaret Dienes (AIP, New York, 1987), pp. 972-1012. W is "W_x" in this reference.

[14]Due to the FEL interaction, the beam will bunch, and $I(\tau)$ will vary on the scale of a signal wavelength. However, he resistive wall wake varies slowly on the scale of a signal wavelength and an average is appropriate.

[15]Alexander W. Chao, *Physics of High Energy Particle Accelerators*, AIP Conf. Proc. No. 105, edited by Melvin Month (AIP, New York, 1983), pp. 353-523. W is "W_1", and τ is "z/c" in this reference.

[16]$k_\beta=2\pi/\lambda_\beta$, where $\lambda_\beta=2\pi(mc^2/e)(\gamma/B_w)$ and $B_w \sim 3$ - 6 kG is the peak wiggler field. In practical units, $\lambda_\beta(cm)\sim 15.2\ \gamma/B_w(kG)$.

[17]S. Bodner, V. K. Neil, and L. Smith, Particle Accelerators **1**, 327 (1970).

[18]This result assumes that the pulse length does not exceed the time for the magnetic field to diffuse through the pipe wall. This constrains the wall thickness, $d >> (c^2\tau_m/4\sigma)^{1/2}\sim 10^{-2}$ cm.

[19]G.J. Caporaso, W.A. Barletta, and V.K. Neil, Particle Accelerators **11**, 71 (1980).

[20]In practical units, with $E=mc^2\gamma$,

$$L_g \approx 1.90\ \mathrm{m}\left(\frac{1\,\mathrm{kA}}{I}\right)\left(\frac{50\,\mathrm{ns}}{\tau}\right)^{1/2}\left(\frac{\sigma}{1\times10^{17}\,\mathrm{sec}^{-1}}\right)^{1/2}\left(\frac{E}{1\,\mathrm{MeV}}\right)\left(\frac{b}{1\,\mathrm{cm}}\right)^{3}\left(\frac{1\,\mathrm{m}}{\lambda_\beta}\right).$$

[21]K. Halbach, Journal de Physique, **44**, 211 (1983).

[22]RWALL divides the beam into a finite number (typically, forty) of slices in τ, and populates each slice with N macroparticles. For Sec. III A and III D, N=1, while for Sec. III B and III C, N=36. The code makes use of a fourth-order gaussian integration in s tailored to the singular integrand, and a fourth-order Runge-Kutta advance in z. As a benchmark, evolution of a fifty nanosecond beam through one-hundred betatron wavelengths, with 3000 numerical steps in z, takes 12.7 minutes on a VAX 8650, with a total error, compared to the "exact" asymptotic result, of under 0.3%, after 4.5 efolds.

[23]N.M. Kroll, P.L.Morton, and M.N. Rosenbluth, IEEE J. Quant. Elec. **QE-17**, 1436 (1981).

[24]The synchrotron period is determined from $\lambda_{synch}=2\pi/k_{synch}$, where

$$k_{synch} = k_w \sqrt{\frac{2a_s a_w}{1 + a_w^2/2}}$$

and $a_w=(eB_w/mc^2)/k_w \sim 6.6\ 10^{-2}\ \lambda_w(cm)B_w(kG)$. The dimensionless rf vector potential, a_s, is related to the microwave power by $P/P_0=(\pi/2)(ab/\lambda_s^2)a_s^2$, where $P_0=m^2c^5/e^2$ = 8.7 GWand λ_s is the signal wavelength ~ 1 - 3 cm. For P=1 GW, and the parameters of Table 1, $a_s \sim 3\times10^{-2}$ and $\lambda_{synch} \sim 2.2$ m. The spread in energy within the ponderomotive bucket is of order $\Delta\gamma \sim (\omega a_s a_w/ck_w)^{1/2}$.

[25]The result of Ref. 12 and that of Appendix A differ in their range of validity. The result of Appendix A assumes $k_s<k_\beta$, while that of Ref. 12 assumes $k_s>2k_\beta$.

[26]V. E. Balakin, A. V. Novokhatsky, and V. P. Smirnov, *Proceedings of the 12th International Conference on High-Energy Accelerators*, edited by F.T Cole and R. Donaldson (Fermi National Accelerator Laboratory, Batavia, Illinois, 11-16 August 1984), pp. 119-120.

[27]It should be added that, for the resistive wall wake potential, energy sweep does not produce true damping. The evolution of the centroid passes through a transient period in which the amplitude actually decreases over some range of z (see Fig. 9). Thereafter, oscillations are asymptotically unbounded, although they grow at a slower rate. D.H. Whittum, "BNS effect for transverse beam break-up of an unbunched beam", (unpublished).

FIG. 1. One superperiod of an FEL Two-Beam Accelerator.

FIG. 2. Center of mass displacement versus τ and z, with no energy spread, for b=1 cm.

FIG. 3. Resistive wall growth at z=100 m, versus pipe radius, with γ constant within the beam and in z.

FIG. 4. Center of mass displacement versus τ and z, with no energy spread, for (a) b=1 cm and (b) b=0.5 cm, for $0<z<10$ m.

FIG. 5. Resistive wall growth at z=100 m, for a sawtooth variation (due to reacceleration) in the average γ, from γ_+ to γ_-, with $(\gamma_+ + \gamma_-)/2=20$, for several values of $\Delta\gamma/\gamma=(\gamma_+ - \gamma_-)/20$. Evidently, periodic acceleration and decceleration increases growth, albeit only slightly.

FIG. 6. Resistive wall growth at z=100 m, versus $\Delta\gamma/\gamma$, the fractional spread in γ *within a beam slice.* The reduction in growth illustrates the effect of Landau damping.

FIG. 7. Resistive wall growth at z=100 m, versus λ_{synch}, with a spread in γ within a beam slice, $\Delta\gamma/\gamma$ =1%. The lack of damping at shorter λ_{synch} illustrates the deleterious effect of rapid synchrotron motion.

FIG. 8. Resistive wall growth at z=100 m, versus $\Delta\gamma/\gamma$, the fractional spread in γ *along the beam.* The reduction in growth illustrates the BNS effect.

FIG. 9. Envelope of the rms center of mass displacement, with BNS damping, corresponding to $\Delta\gamma/\gamma$= -4.0%, (an rms sweep of about -1%), to be compared to Fig. 2.

FIG. A1. Comparison between analytic and numerical results for asymptotic growth of the resistive wall instability, at z=100 m, (a) *without* the corrections indicated in Eq. (A.11) and (b) *with* the corrections.

FIG. B1. Comparison between analytic and numerical results for the effect of synchrotron motion on Landau damping of the resistive wall instability. This is Fig. 7, with the analytic result superimposed.

Table I. FEL TBA design parameters considered for the examples.

λ_w=wiggler wavelength ~ 27 cm
λ_β=betatron wavelength ~ 1 m
λ_{synch}=synchrotron period ~ 2 m
I=beam current ~ 3 kA
σ=wall conductivity ~ $1x10^{17}$ sec^{-1}
b=pipe radius ~ 0.5 - 2 cm
$\gamma=E/mc^2$ ~ 20
τ_m=pulse length ~ 50 ns
z_m=overall TBA length~100 m
L=TBA period length ~ 1.30 m

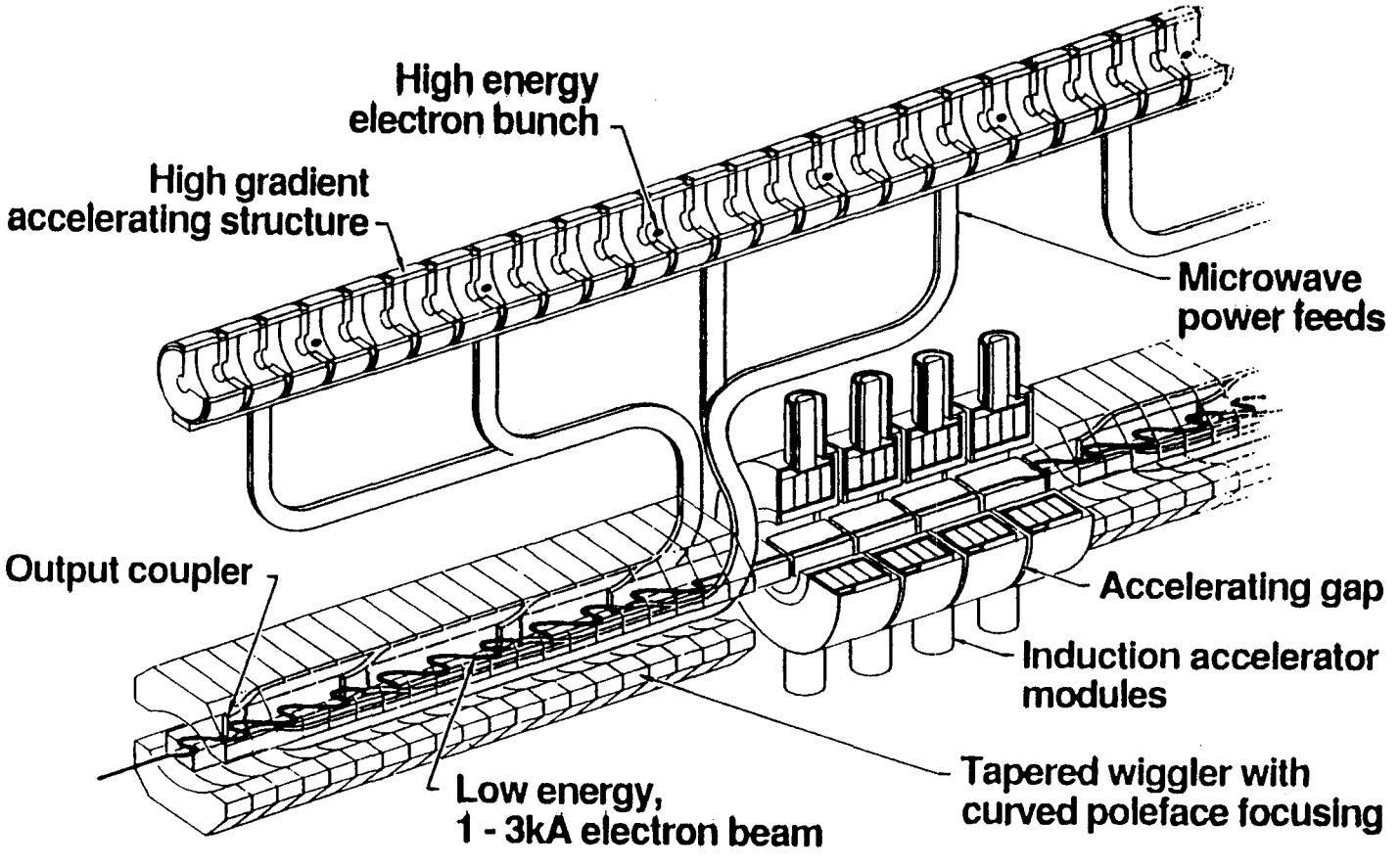
High energy
electron bunch
High gradient
accelerating structure
Microwave
power feeds
Output coupler
Accelerating gap
Induction accelerator
modules
Tapered wiggler with
curved poleface focusing
Low energy,
1 - 3kA electron beam

FIG. 1

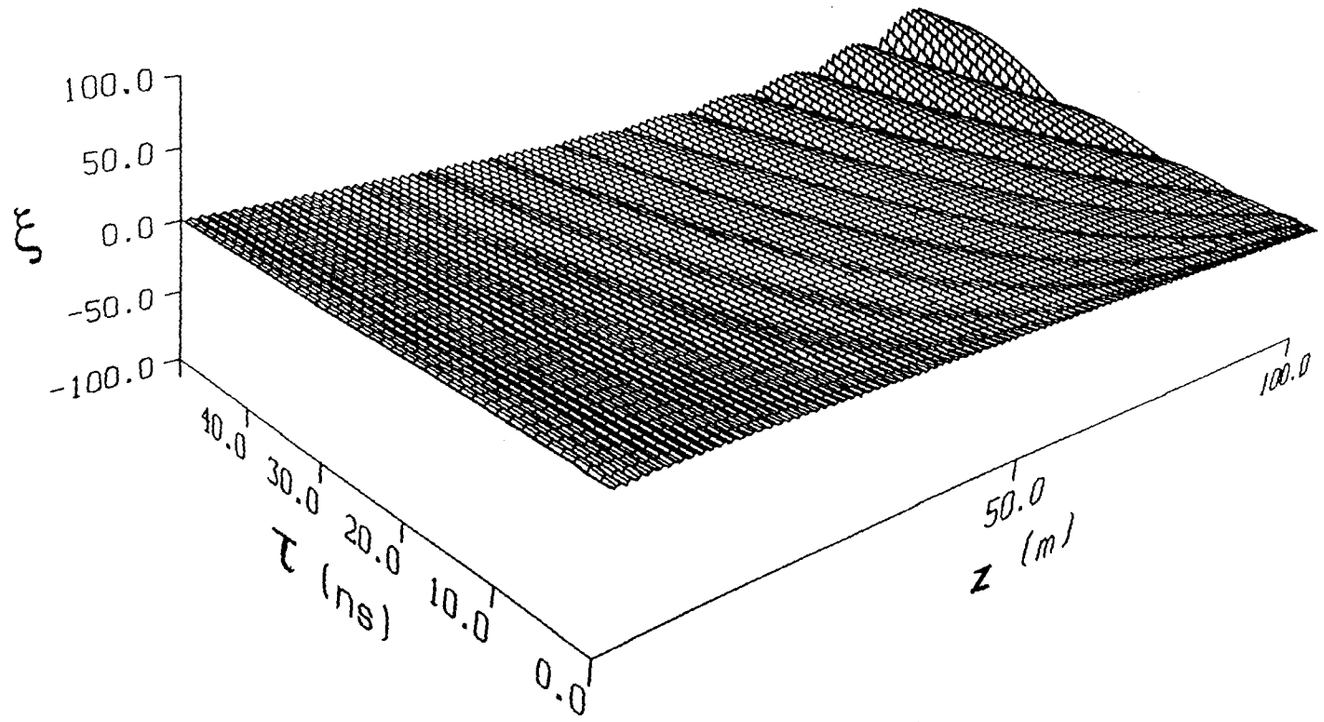

FIG. 2

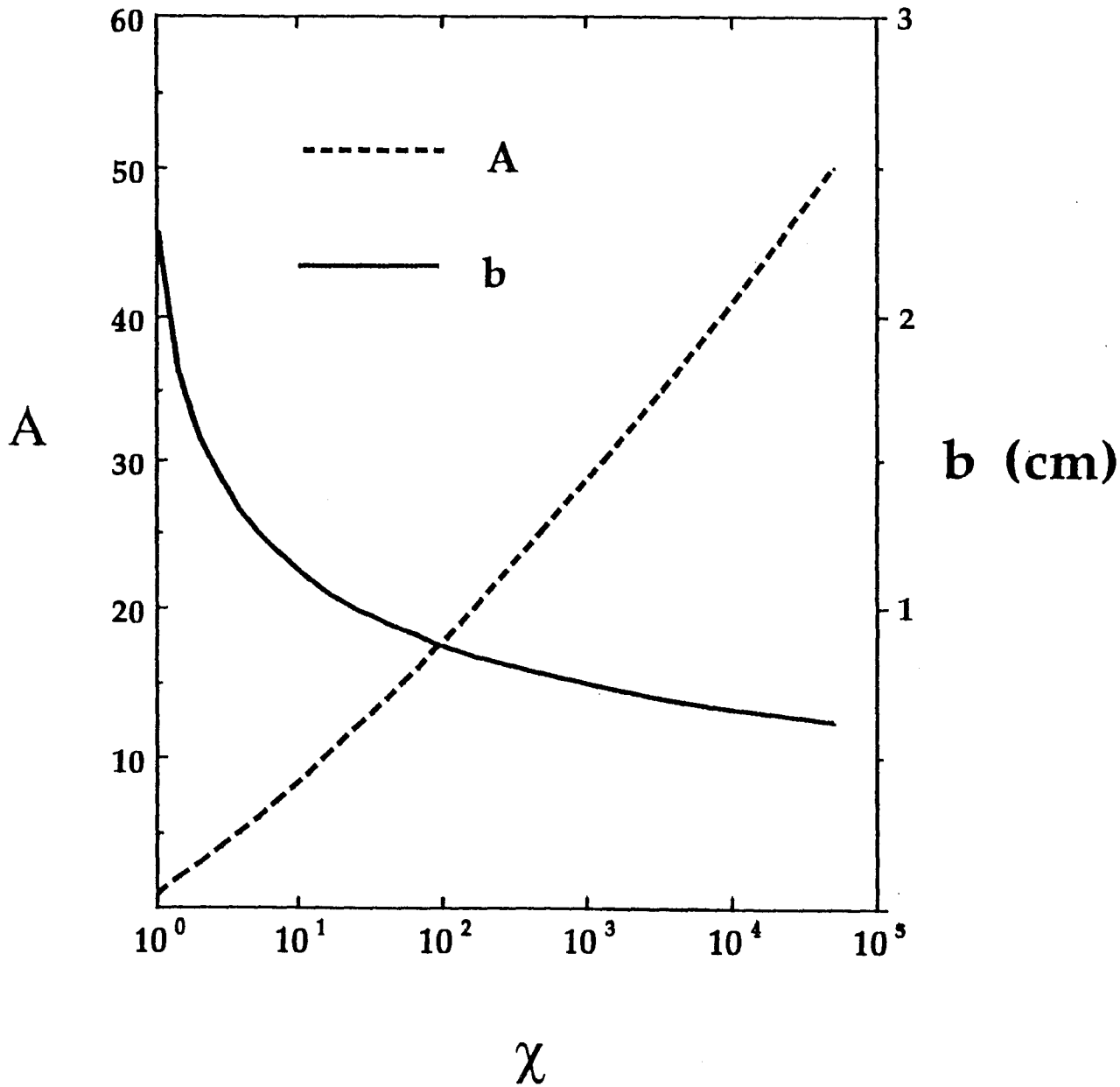

FIG. 3

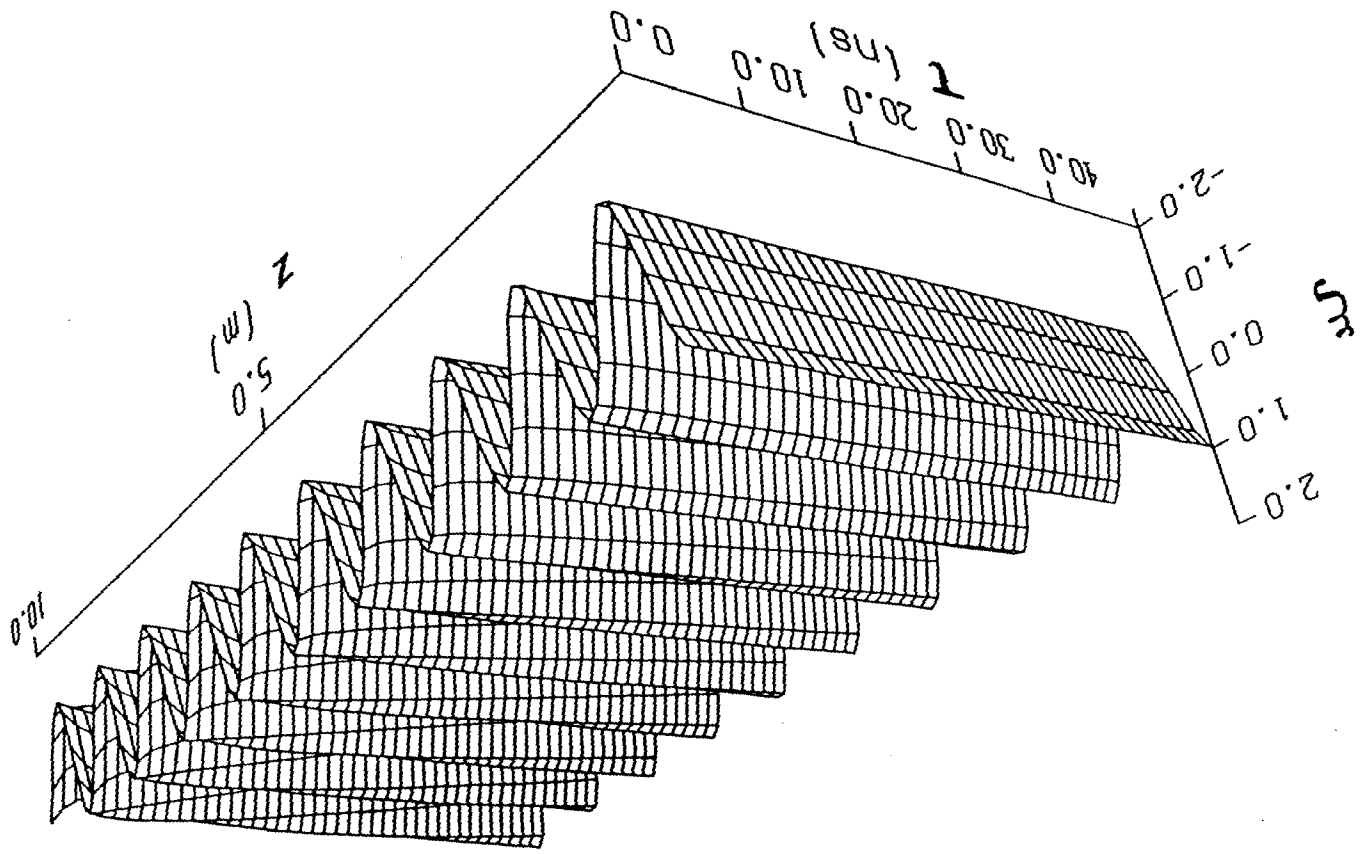

FIG. 4(a)

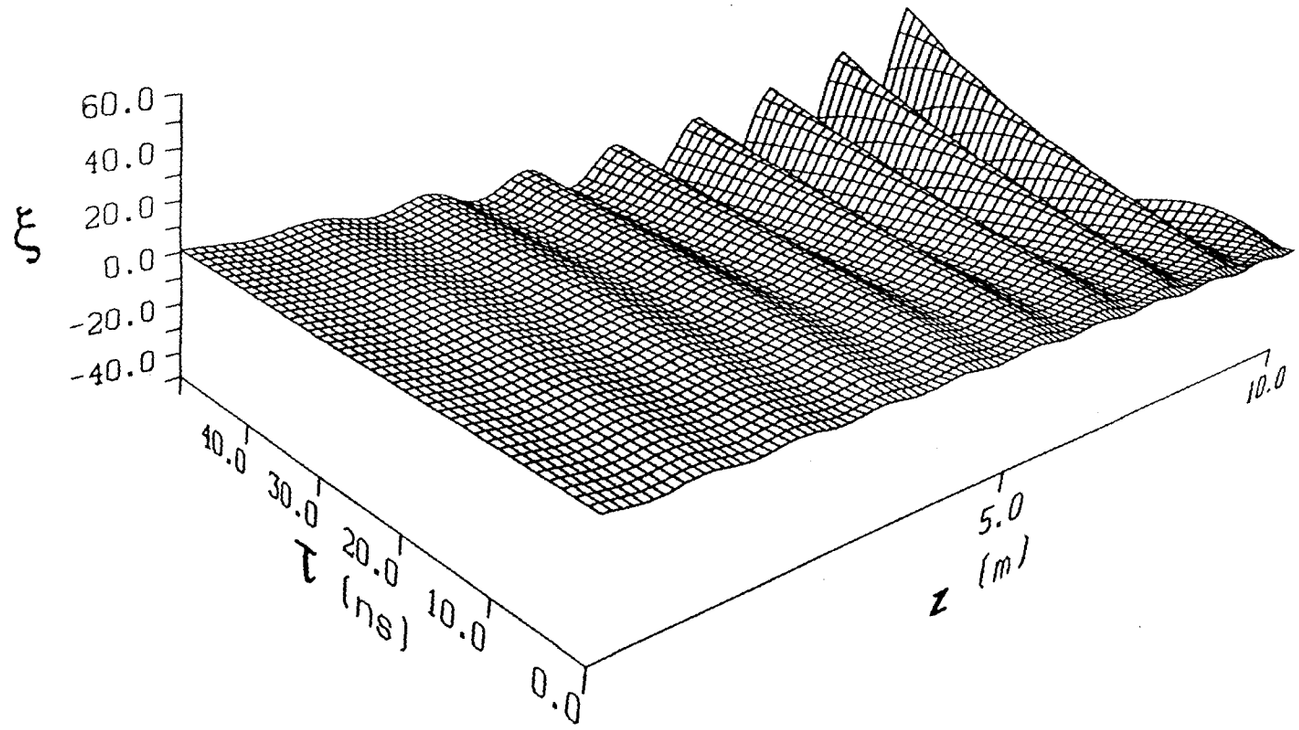

FIG. 4(b)

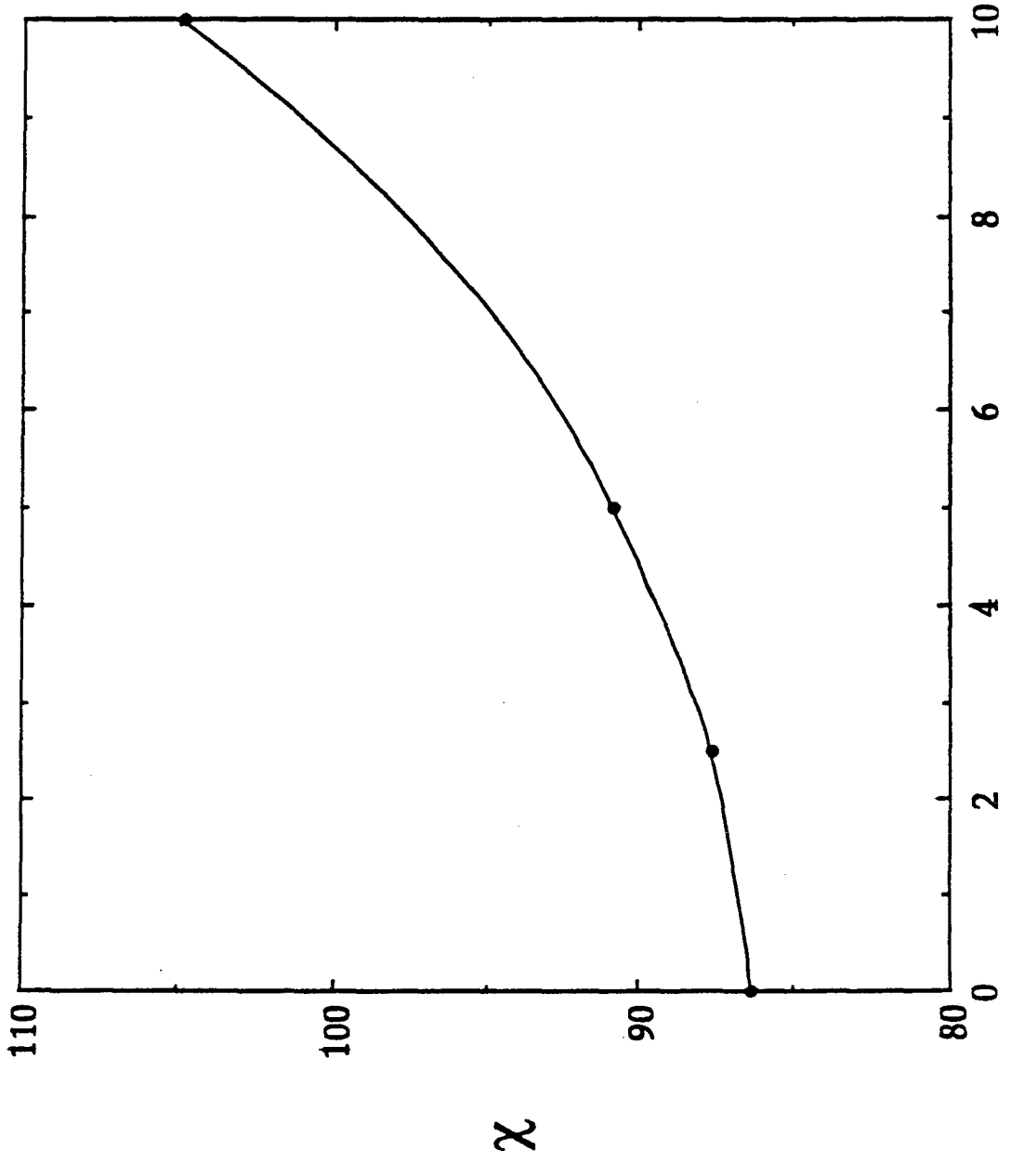

FIG. 5

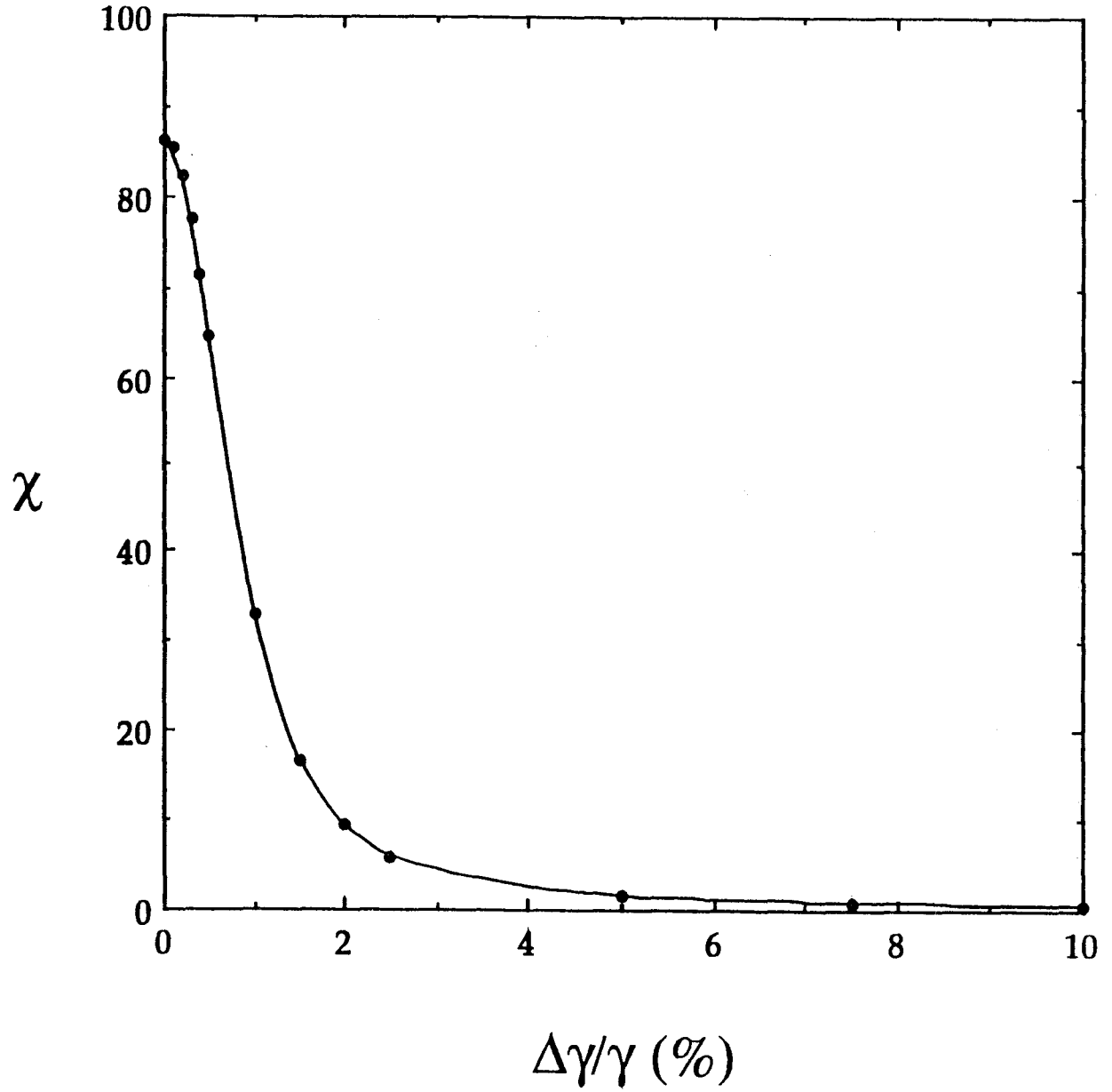

FIG. 6

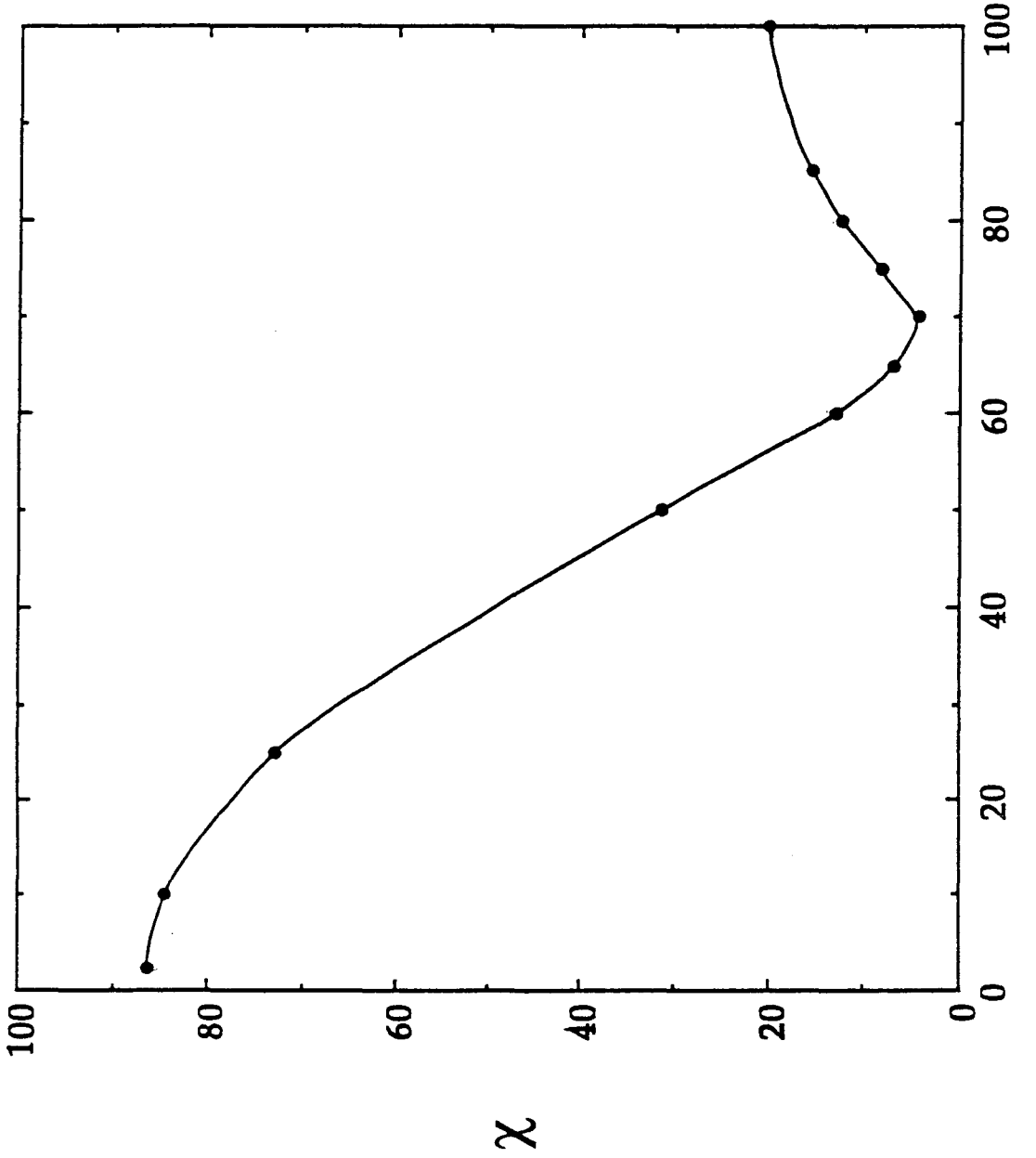

FIG. 7

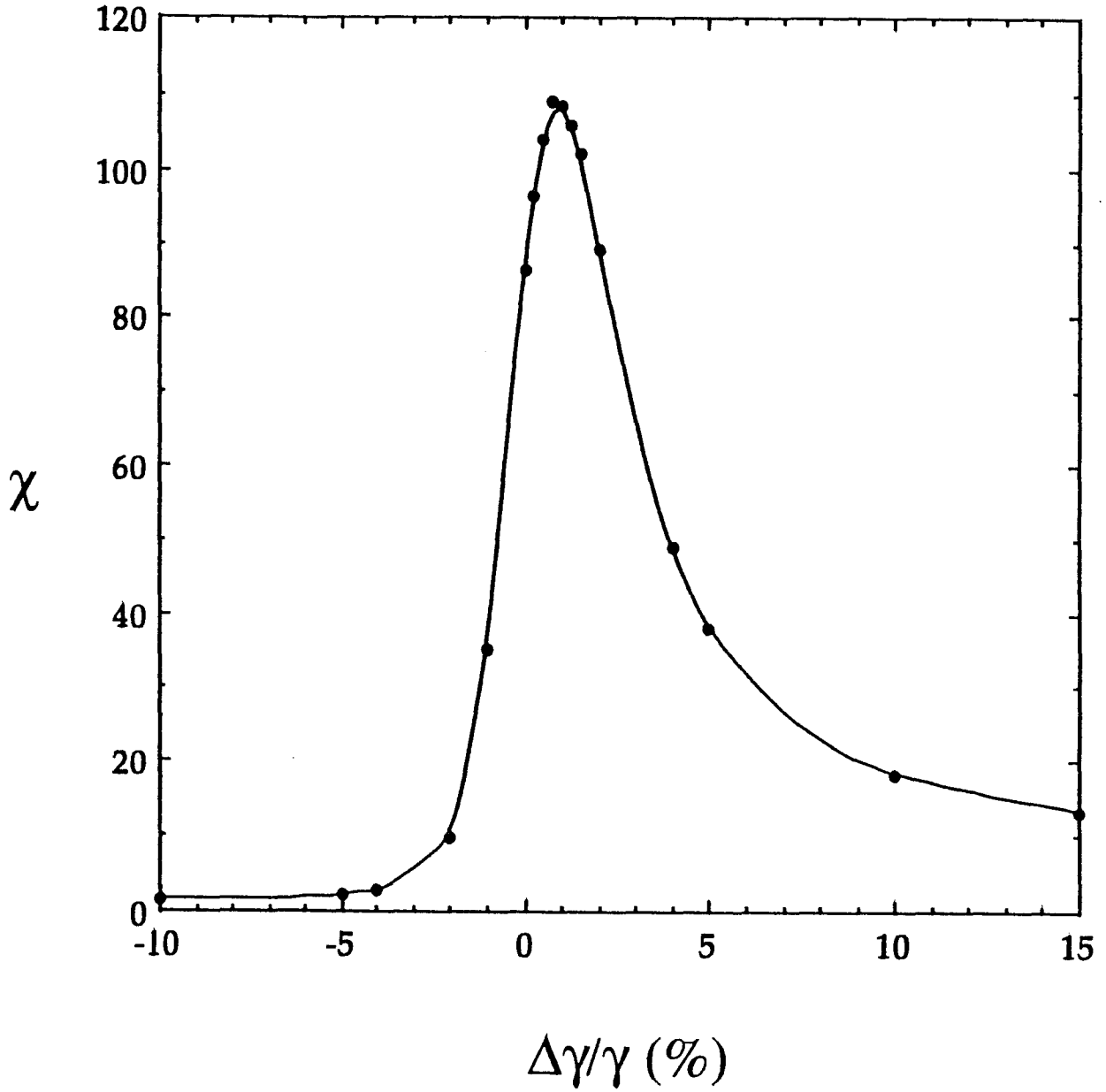

FIG. 8

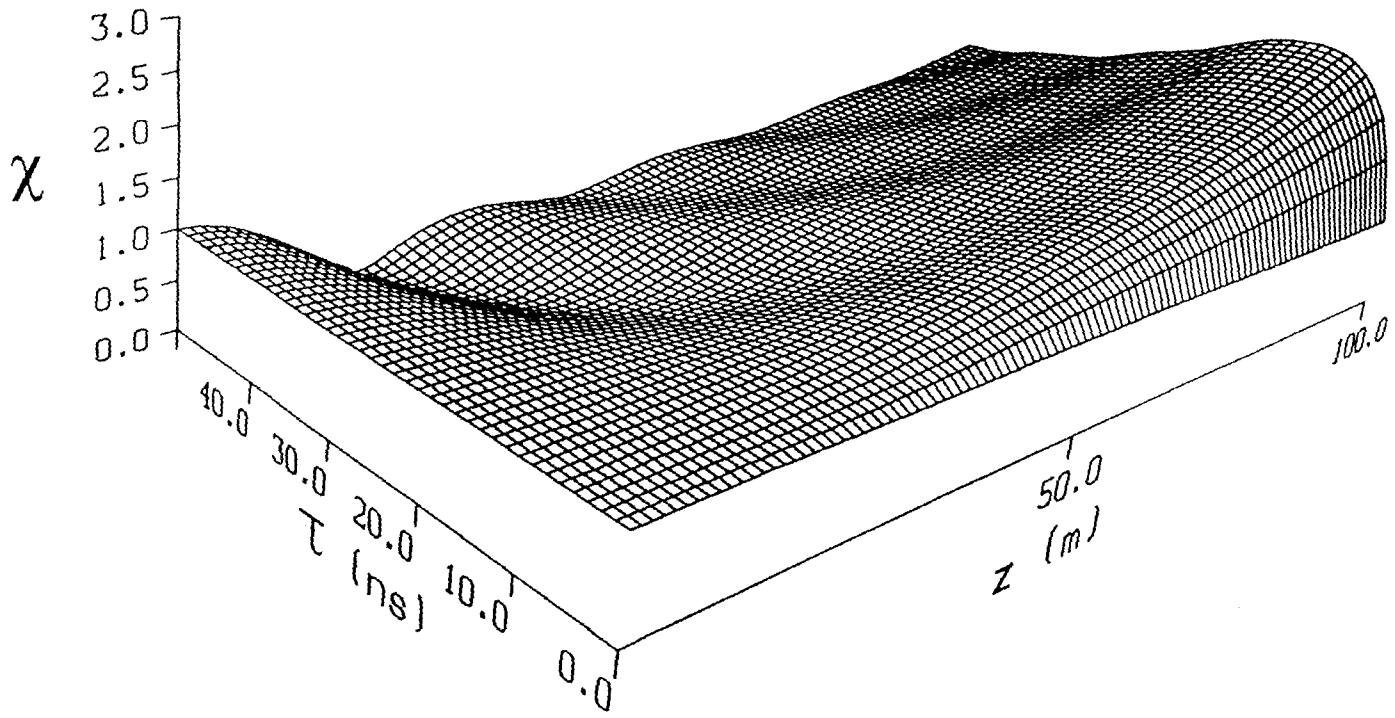

FIG. 9

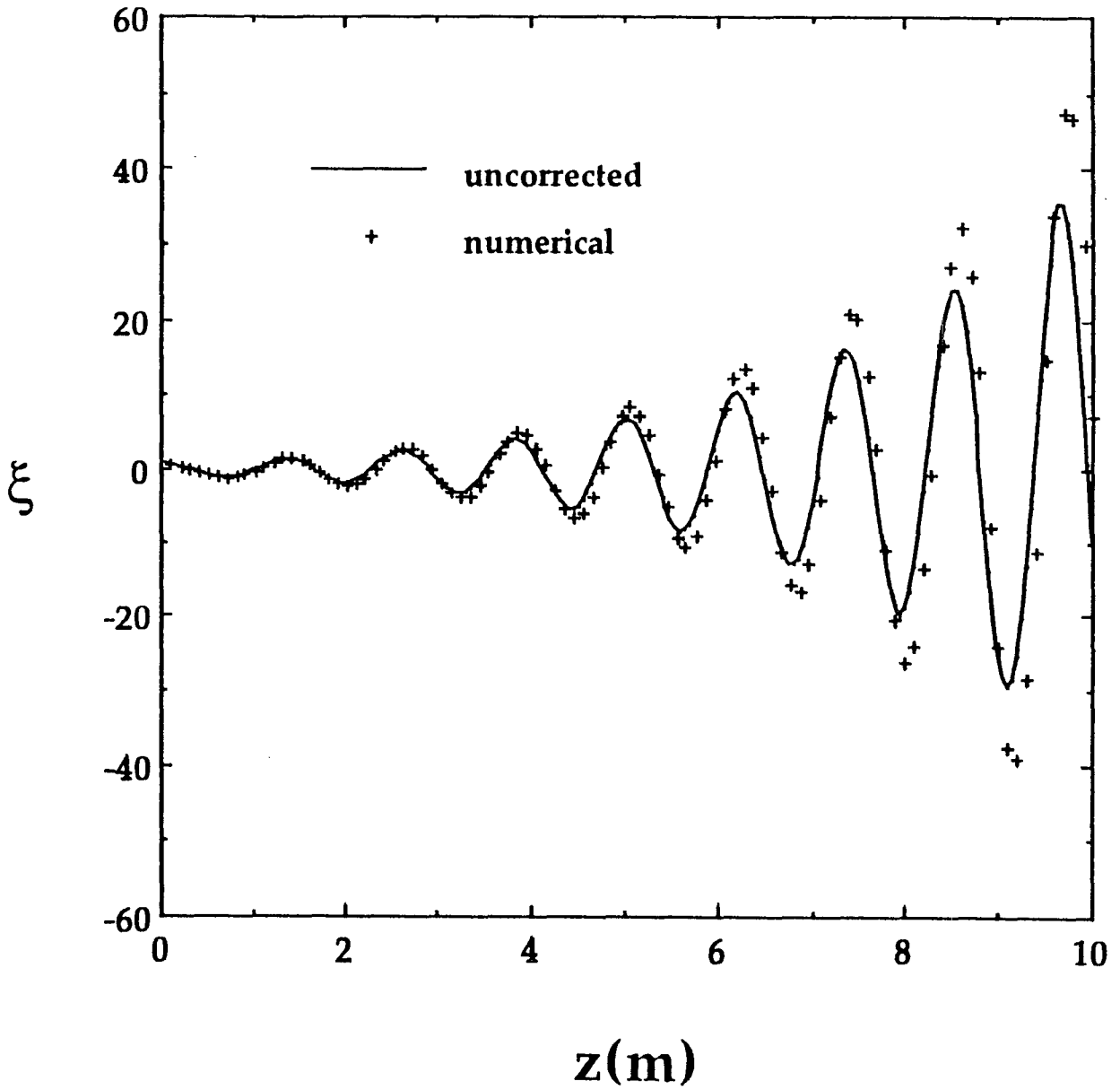

FIG. A1(a)

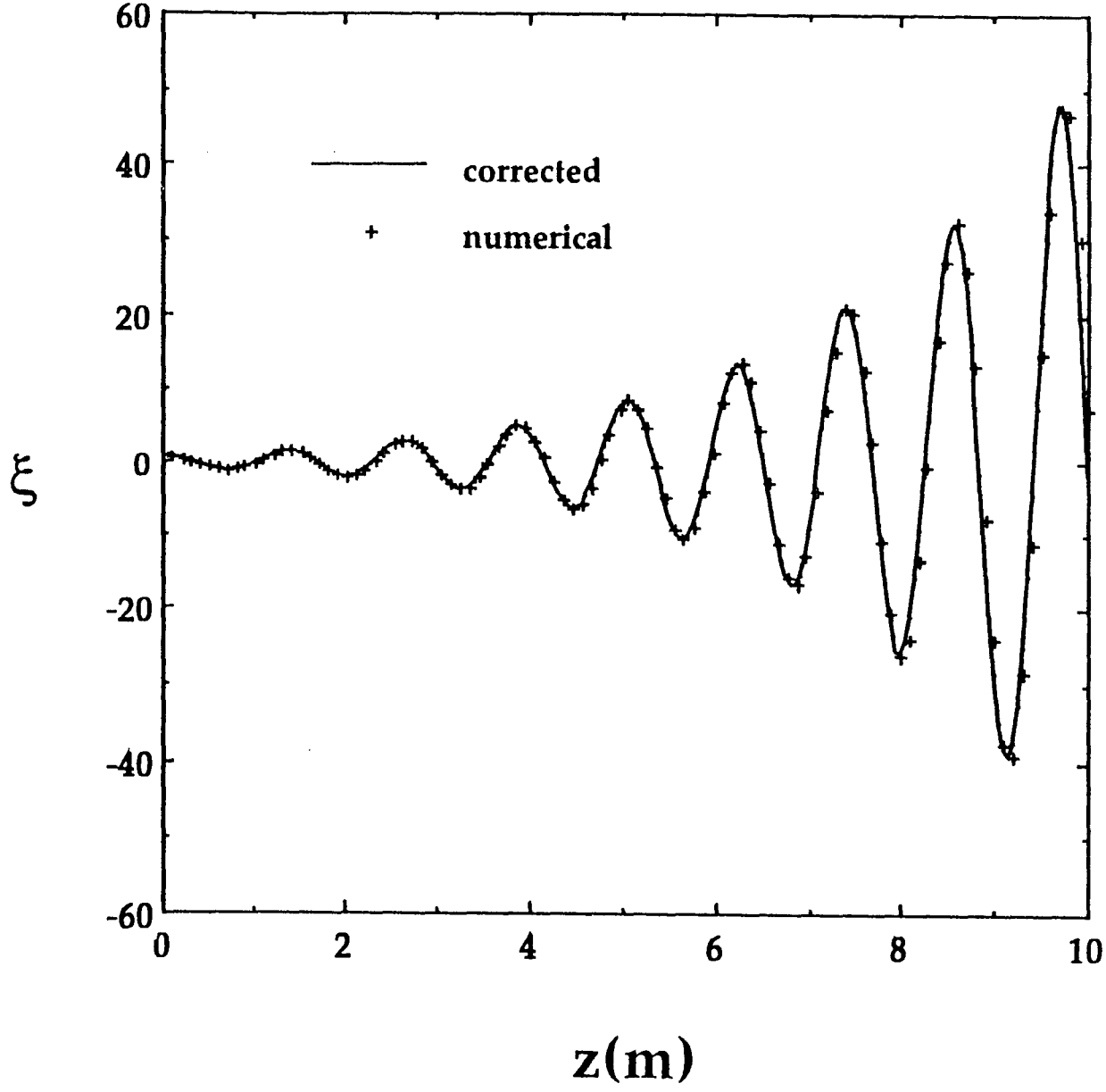

FIG. A1(b)

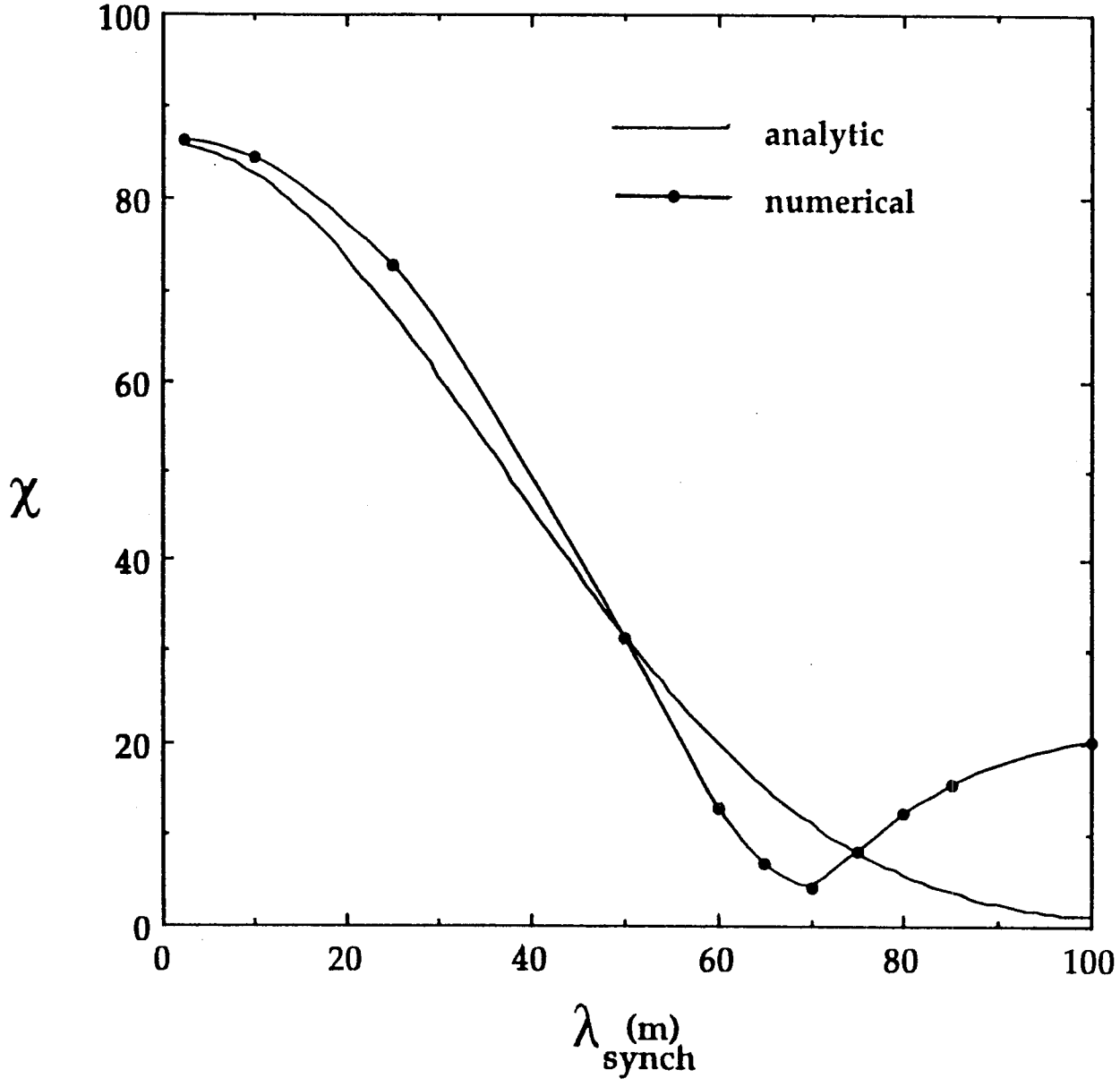

FIG. B1